© Crown Copyright, 2016

J. Am. Soc. Mass Spectrom. (2016) 27:1411–1418
DOI: 10.1007/s13361-016-1401-5

RESEARCH ARTICLE

Systematic Temperature Effects in the Argon Cluster Ion Sputter Depth Profiling of Organic Materials Using Secondary Ion Mass Spectrometry

Martin P. Seah, Rasmus Havelund, Ian S. Gilmore

Surface and Nanoanalysis, National Physical Laboratory, Teddington, Middlesex, TW11 0LW, England, UK

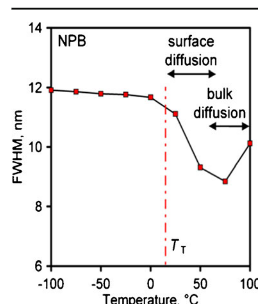

Abstract. A study is presented of the effects of sample temperature on the sputter depth profiling of two organic materials, NPB (*N,N′*-Di(1-naphthyl)-*N,N′*-diphenyl-(1,1′-biphenyl)-4,4′-diamine) and Irganox 1010, using a 5 keV Ar_{2000}^+ cluster ion beam and analysis by secondary ion mass spectrometry. It is shown that at low temperatures, the yields increase slowly with temperature in accordance with the Universal Sputtering Yield equation where the energy term is now modified by Trouton's rule. This occurs up to a transition temperature, T_T, which is, in turn, approximately $0.8T_M$, where T_M is the sample melting temperature in Kelvin. For NPB and Irganox 1010, these transition temperatures are close to 15 °C and 0 °C, respectively. Above this temperature, the rate of increase of the sputtering yield rises by an order of magnitude. During sputtering, the depth resolution also changes with temperature with a very small change occurring below T_T. At higher temperatures, the depth resolution improves but then rapidly degrades, possibly as a result first of local crater surface diffusion and then of bulk inter-diffusion. The secondary ion spectra also change with temperature with the intensities of the molecular entities increasing least. This agrees with a model in which the molecular entities arise near the crater rim. It is recommended that for consistent results, measurements for organic materials are always made at temperatures significantly below T_T or 0.8 T_M, and this is generally below room temperature.

Keywords: Ar ion clusters, Delta layers, GCIB, Irganox 1010, Multilayers, OLEDs, Organic layers, NPB, Sputtering yield, Temperature

Received: 8 January 2016/Revised: 30 March 2016/Accepted: 31 March 2016/Published Online: 22 April 2016

Introduction

Sputter depth profiling using surface analytical techniques provides a strong capability for spatially resolved chemical analysis. Since the introduction of cluster sputter ion sources, this has become increasingly important for the analysis of organic materials, including organic electronic devices and biological specimens where the distribution of materials such as lipids and pharmaceutical molecules can be imaged with sub-micrometer resolution using secondary ion mass spectrometry (SIMS) [1–7]. For the sputter depth profiling of organic materials, the sputtering ion of choice today is the argon cluster ion [8]. Argon cluster ions are generally preferred because they generate profiles in which there is little degraded material or deposit from the ion beam remaining on, or in, the surface after the ion impact. This means that for 1-beam or 2-beam SIMS profiles, the sputtering rates are fairly uniform with dose and that the measured SIMS spectrum changes little with dose. These improvements are clearly seen in the comparison between data using C_{60}^+ primary ions [9] and argon clusters [10] in the depth profiles of Irganox 3114 delta layers in Irganox 1010. Careful studies of such samples show that sample rotation is beneficial [3], achieving depth resolutions measured by the full width at half maximum (FWHM) as low as 4 nm at depths up to 300 nm.

The above results all confirmed the early promise indicated by Lee et al. [11] for depth profiling with argon gas cluster ion beams (GCIBs). In that study, and the study by Shard et al. [9], detailed measurements of the sputtered topography were made using atomic force microscopy (AFM) and it was shown that the interface resolution for the delta layers in Irganox 1010 was dominated by the roughening that developed but that also the asymmetric profile for each delta layer, described by the function of Dowsett et al. [12], fitted the height populations of the sputter-roughened surfaces. It is relevant to note that Shard

Correspondence to: Martin P. Seah; *e-mail:* martin.seah@npl.co.uk

et al. [9] state that AFM images recorded for Irganox 1010 showed, 1 d later, that the roughness had reduced. This demonstrated that surface relaxation can occur during experimental timescales for these organic materials at room temperature. It was suggested that storage at low temperatures may preserve the sputtered surface microstructure. Green et al. [13] showed gross amounts of dewetting can occur for Irganox 1010 films less than 5 nm thick after 13 days at room temperature, whereas phenylalanine seemed very stable over longer periods at this thickness [14]. In more recent work, Seah [15] calculates that significant molecular movement by surface diffusion is possible for some organic materials at room temperature. This is, of course, not wanted in most analytical situations.

Besides the effects on sample stability, the sample temperature is also an important analytical condition. In a detailed survey of the SIMS of polymers and related materials by cluster primary ions, Mahoney [16] notes that at high temperatures, polymers show ion-induced depolymerisation and, at low temperatures, reduced cross-linking. Below the glass transition temperature, T_g, free radicals becomes trapped and their reaction rate is reduced. Mahoney et al. [17] show, for poly(methylmethacrylate) (PMMA) sputtered by 5 keV SF_5^+, that the depth resolution was best at –75 °C, good at the higher temperature of 125 °C but was very poor at the commonly used intermediate temperature of 25 °C. AFM studies confirmed that the roughness was worst at 25 °C but the depth profiles seem much poorer than the roughness would indicate (maybe adventitious annealing had occurred prior to the AFM measurements). Along with the improved resolution at 125 °C was an almost doubled sputtering rate attributed to ion beam-induced depolymerisation [18]. Residual gas analysis showed enhanced methylmethacrylate monomer present [19] that more or less correlated with the enhanced sputtering rate. Recent studies of the effect of the reduction in molecular weight on sputter yields confirm, in detail, that strong enhancement [20, 21] of the sputtering yield will occur for the monomer. In a similar manner, Möllers et al. [22], in a study of PMMA sputtered by 10 keV C_{60}^+, find that the depth resolution for 200 nm thick films was better at elevated and reduced temperatures and, again, worst at 20 °C. The sputtering yield had doubled at 140 °C and tripled at 180 °C. All these effects are discussed clearly with the models in the review by Mahoney [16] and relate to polymers, their cross linking, depolymerisation, and other polymer-related behavior.

In the present work, we are involved with organic materials that have many similarities with, and importantly many differences to, polymers, to see how the behaviors compare. Using carefully constructed model systems, we conduct a study of the effect of the sample temperature in argon cluster sputter depth profiling of molecular samples. The materials studied are *N,N′*-Di(1-naphthyl)-*N,N′*-diphenyl-(1,1′-biphenyl)-4,4′-diamine (molecular weight 588.74, $C_{44}H_{32}N_2$, called NPB), and Irganox 1010 (molecular weight 1177.63, $C_{73}H_{108}O_{12}$), both of which have been used extensively in SIMS studies. To evaluate the sputtering rates and effects on depth resolution, these samples contain delta layers of Alq3 tris(8-hydroxyquinolinato)aluminium (molecular weight 459.4, $C_{27}H_{18}AlN_3O_3$) and Irganox 3114 (molecular weight: 784.08, $C_{48}H_{69}N_3O_6$), respectively. Of course, none of these organic materials is a polymer and, thus, do not depolymerize.

Experimental

NPB and Alq3 were purchased from Sigma-Aldrich. Irganox 1010 and Irganox 3114 were sourced from CIBA (Macclesfield, UK). Organic multilayer samples were created by alternate evaporation of the two relevant materials onto a clean Si wafer substrate (10 mm × 10 mm) in a vacuum coater (AUTO306; Edwards, Crawley, UK). In the NPB sample, four delta layers of Alq3 with nominal thicknesses of 1 nm were deposited between NPB layers of 50 or 100 nm nominal thicknesses to construct a multilayer with Alq3 delta layers centered at 42.5, 90.1, 184.4, and 278.5 nm depths. In the Irganox 1010 sample, delta layers of Irganox 3114 with nominal thicknesses of 1 nm were deposited between Irganox 1010 layers to obtain a structure similar to that of the NPB sample but with the layers centered at 47.1, 94.75, 188.95, and 283.1 nm. The layer thicknesses were monitored during deposition by in-situ quartz crystal microbalance (QCM) measurements. The relationships between the QCM thickness values and the deposited amount of material, as measured by spectroscopic ellipsometry (M2000DI; Woollam Co., NE, USA), were established prior to sample construction. Samples were stored at 5 °C prior to use.

SIMS sputter depth profiling of the multilayer samples was conducted using an ION-TOF TOF.SIMS IV (ION-TOF GmbH, Muenster, Germany) operated in a 2-beam mode. A 5 keV Ar_{2000}^+ ($\Delta m/m = 0.3$) sputtering beam with an average current of 0.60 nA was set to sputter a 500 μm × 500 μm area of the sample. The central 200 μm × 200 μm of the sputter crater was analyzed using a 25 keV Bi_3^+ beam at an average DC current of 0.10 pA. The ‘interlaced’ analysis mode, where argon cluster sputtering takes place between each Bi_3^+ analyzing ion pulse impact (5 kHz), was selected. The Bi_3^+ dose in each cycle was less than 0.2% of the Ar GCIB dose to ensure that it has negligible effect on the Ar GCIB sputtering. A heating/cooling stage (ION-TOF GmbH) was used for sample temperature control. Prior to analysis, the samples were cooled to below –100 °C and negative secondary ion depth profiles were recorded for every 25 °C rise in temperature. An interval of at least 10 min was allowed for the sample temperature to settle after each step increase in temperature. Selected characteristic ions for the delta layers were the Irganox 3114 large fragment ion, $C_{33}H_{46}N_3O_5^-$ at *m/z* 564.3, for the Irganox 1010 sample and the 8-hydroxyquinoline ligand ion, $C_9H_6NO^-$ at *m/z* 144.0, for the NPB sample.

Results and Discussion

Sputtering Yields

The depth profiles for the marker layers in both the NPB and Irganox 1010 samples are very similar and are illustrated in Figure 1a and b, respectively. The plotted points are the measured data and the continuous line is a fit using Dowsett et al.'s function [12]. This function involves, for each delta layer, a Gaussian roughening term of characteristic, σ, convolved with an exponential rising edge of characteristic λ_u, often associated with an information depth, and an exponential decay edge of characteristic, λ_d, often associated with atomic mixing. Here, we do not associate these parameters with identified physical phenomena but note that the whole function provides a very good description for delta layer profiles in organic materials. The centroid of this function is given by the center of the Gaussian part minus λ_u, plus λ_d [23]. It is this centroid that we shall use to define the depth sputtered for determining the sputtering rates. We shall assume that the delta layers sputter at the same rate as the matrix [24].

Thus, we get the doses appropriate to the depths of each layer as illustrated for the Irganox sample shown in Figure 2. The straight line is a fit for the depth (nm) = 1.27 + 27.11D, where D is the relevant dose in ions/nm^2. Directly from this, the volume yield per primary ion is 27.11 nm^3. The offset of 1.27 nm could indicate a slightly faster sputtering rate at the start but has contributions from the effect of the analysis beam species and its energy. This offset is not unexpected but it is not as great as with many ion sources since there is little damage or deposit to reduce the sputtering rate from that found initially. The standard deviation of the scatter about the line is 0.42 nm. The sputtering yields for many temperatures are shown in Figure 3 for NPB and Irganox 1010. The data at 25 °C are very consistent with previous data [25, 26]. Note that the Irganox 1010 yield data go to 50 °C; however, at 50 °C the delta layers were no longer clearly visible, although the total Irganox 3114 signal was unchanged, and in this single instance the sputtering yield was therefore estimated from the dose to profile to the Si substrate. The resolution at this interface was good but there may be enhanced sputtering at the interface region leading to a yield value some 1% or 2% too high [27].

The sputtering yields as a function of temperature show a steady increase up to around room temperature and then a more rapid rise. In the linear region below the rapid rise, we may write

$$Y(T) = Y(273)\ [1 + \beta(T - 273)] \qquad (1)$$

where T is the sample temperature in Kelvin. $Y(T)$ is the yield volume per ion that occurs at temperature T but is measured from the thicknesses at room temperature (i.e., we do not allow for, or measure, the increase in layer thicknesses with temperature).

Although the temperature dependence of the depth resolutions have been measured for polymers, the temperature dependence of the sputtering yields for organics using Ar GCIBs have not. The effect of temperature on sputtering yields has, however, been studied for metals using monatomic Ar ions. The energy deposition processes for monatomic and GCIBs are quite different but the material-to-material dependence of the sputtering yield is dominated by the material binding energy, U, in both cases [25, 28, 29]. This is shown nicely in the study of Yamada et al. [30]. Data for polycrystalline metals using monatomic Ar ions are given by Nelson [31], and by Carlston et al. [32], as shown in Table 1. Eckstein [33], in considering such systems, notes that collisional sputtering should not depend on temperature, at least for randomized target structures, as long as the surface binding energy is constant. Most theoretical studies of the effect of temperature on sputtering in metals are concerned with channelling theory and the effects of collisions down the crystal directions; however, there are at least two other temperature-dependent parameters in the binary collision sputtering theory: the binding energy and the atomic volume, a^3 [28, 29]. The binding energy will decrease, causing a rise in yield, whereas the atomic volume will increase, leading to a small fall in yield [28, 29]. Note that for elements, the yield is expressed as atoms sputtered per primary ion, whereas for organic materials we use the volume (measured at room temperature) sputtered per primary ion. For the a^3 term, the

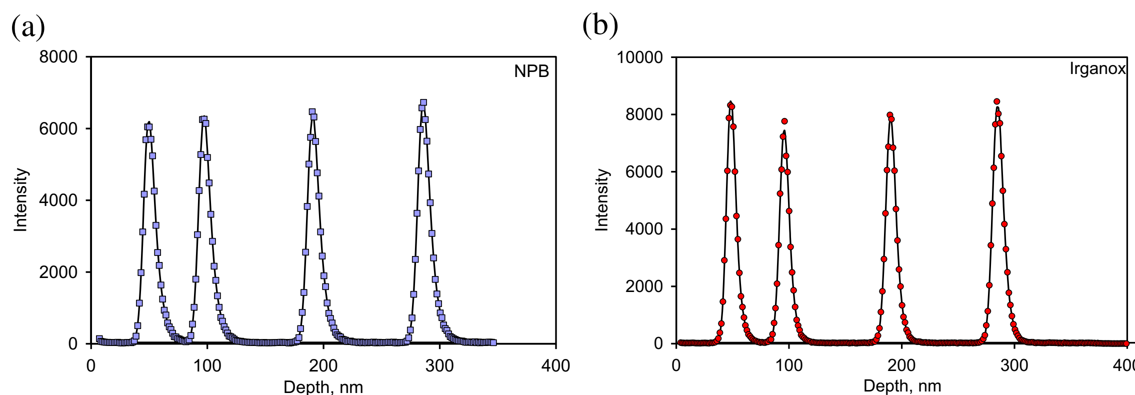

Figure 1. Depth profiles for delta layers at –100 °C sputtered by 5 keV Ar_{2000}^+ and measured using 25 keV Bi_3^+, **(a)** Alq3 in NPB monitoring the $C_9H_6NO^-$ secondary ion at 144.0 Da, and **(b)** Irganox 3114 in Irganox 1010 monitoring the $C_{33}H_{46}N_3O_5^-$ secondary ion at 564.3 Da

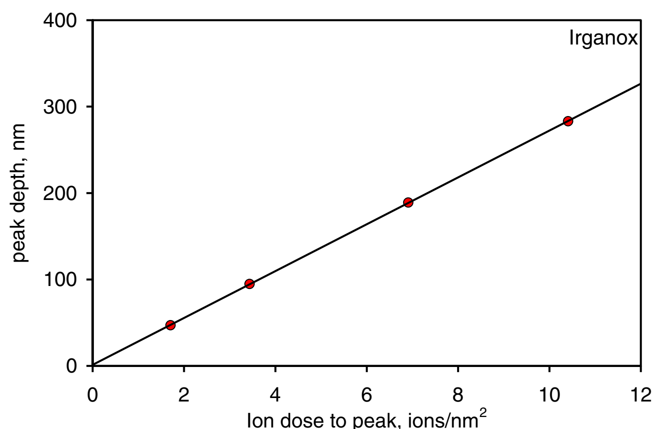

Figure 2. Dose to sputter to each of the four delta layer depths in Irganox 1010 monitoring the $C_{33}H_{46}N_3O_5^-$ secondary ion at 564.3 Da

sputtering yield in atoms for monatomic sputtering is proportional to a^{-3} and so the volume sputtered is independent of a, i.e., the volume sputtered at elevated temperatures is predicted to be unchanged when measured at that temperature so, at room temperature, there will be a small reduction.

Nelson [31] developed a thermal spike model in which the thermal energy per target atom is added to the energy deposited in the spike volume and this, he felt, led to the rapid rise part of the sputtering yield at the higher temperatures. A quite contrary view is expressed by Besocke et al. [34] who, in careful studies of Ag sputtered by 8 keV Ar^+ and Xe^+ ions, find that the transition temperature arises from the onset of evaporation and that there is no significant thermal spike sputtering involved.

Before discussing the ion spectra, it is worth comparing the results of Nelson's early studies on metals with the present study on organic materials. There are two sputtering yield regimes to consider: (1) the low temperature relative yield gradient, β from Equation (1), and (2) the temperature, T_T, at which a transition to the faster sputtering rate occurs.

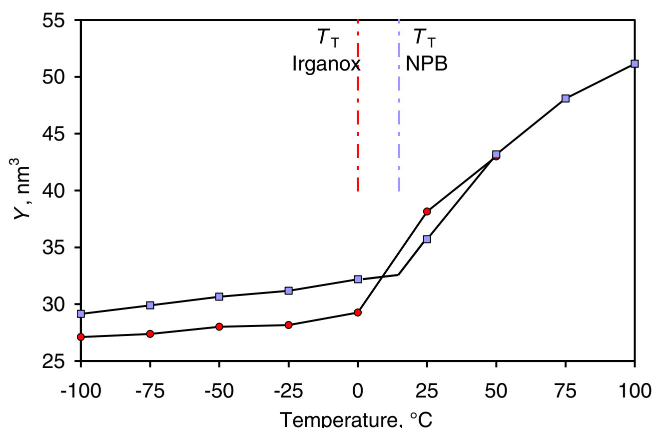

Figure 3. Sputter yield volumes for NPB and Irganox 1010 sputtered by 5 keV Ar_{2000}^+ as a function of the sample temperature with the transition temperatures

The relative rates of rise of the yield, β, for NPB and Irganox 1010, for temperatures below 0 °C are 9.2 × 10^{-4}/K and 7.0 × 10^{-4}/K, respectively. These, as well as Nelson's values and Besocke et al.'s values, are plotted in Figure 4a. Considering the two effects noted above, for the sputtering of elements by monatomic ions, the yield depends inversely on both the binding energy of the material, U, and the atomic volume, a^3, for monatomic ions in binary collision theory [28, 29], and also, for U, for elements sputtered by argon gas clusters [25, 30]. The binding energy is deduced from the heat of vaporization that reduces with temperature at a rate governed by the entropy of evaporation. For many materials, this entropy is 10.5 k per atom or molecule, where k is the Boltzmann constant, and this rule is known as Trouton's rule [35], which is good for many materials [36] and organic compounds with a low degree of order [37, 38]. The fractional change in U is thus 10.5 k/U and is shown by the dashed red line in Figure 4a. Whilst this reduction in U increases the sputtering yield, the increase in atomic spacing may reduce the yield. This reduces β by approximately three times the linear expansion coefficient. This coefficient is not known for NPB or Irganox 1010 but here we use a value of 25 × 10^{-6}/K as a typical value for Nelson's materials at the higher temperatures [39]. Inclusion of this is shown by the thin red line. However, we do not know the values of U for NPB and Irganox 1010. We can estimate U from the fact that we evaporate both materials in vacuo at ~400 °C and that their vapor pressures at room temperature are sufficiently low for them to be stable. Thus U ~ 1 eV. A slightly better estimate of U may be made via Walters et al.'s Equations 2 and 3 [40], with Trouton's rule, to give U(NPB) = 1.0 eV and U(Irganox 1010) = 1.3 eV. These are the values used in Figure 1a. The experimental data support this, showing that the temperature dependence of U describes the dominant source of the yield change for NPB and Irganox 1010 below the transition temperature, T_T. More weakly bonded materials, not unsurprisingly, will exhibit a greater fractional rise, β, in the sputtering yield.

Materials with weak bonds will have higher vapor pressures, sputter more easily, and have a lower melting temperature, T_M. This is most readily seen in the data of Cristaudo et al. [20], and Seah [21], where the yield rises as the molecular weight and, hence, T_M, both fall. In Figure 4b, the sputtering transition temperature, T_T, is plotted as a function of T_M where these temperatures are in Kelvin. For organic materials, T_M is generally known, whereas U and other parameters, which may be more closely related to T_T, are not. The correlation shown by the solid line with $T_T \simeq 0.8\ T_M$ is reasonable and indicates that many interesting organic materials like these with T_M < 100 °C may well have T_T values significantly below room temperature. Figure 4c shows T_T versus U/k where U has been taken as 1 eV for NPB and 1.3 eV for Irganox 1010. The overall correlations above seem reasonable but it must be remembered that Nelson's [31] and Besocke et al.'s [34] data are for monatomic primary ions, whereas the data for the organics use 5 keV Ar_{2000}^+ primary ions. Although the physics involved in the two cases is quite different, the plots in Figure 4b and c clearly indicate that more

Table 1. Temperature Coefficient for the Rise in Sputtering Yield

Target material	Primary ion	β, relative rise in yield/K.10^{-4}	Ref
Cu		0.6	
Zn		5.1	
Ag	45 keV Xe^+	1.0	31
Au		0.5	
Bi		2.2	
Al		0	
Cu		0.72	
Mo	5 keV Ar^+	4.0	32
W		4.3	
Ta		6.0	
Ag	8 keV Ar^+	1.1	34
Ag	8 keV Xe^+	1.8	34

weakly bonded materials, unsurprisingly, will exhibit a lower transition temperature.

The above results all appear to be of high consistency, indicating that effects for NPB occur at about 15 °C higher temperatures than for Irganox 1010 and that the yields rise at 9 × 10^{-4} K^{-1} and 7 × 10^{-4} K^{-1} up to 15 °C for NPB and 0 °C for Irganox 1010, respectively; then at a significantly higher rate at higher temperatures. The relative rate of rise below T_T is similar

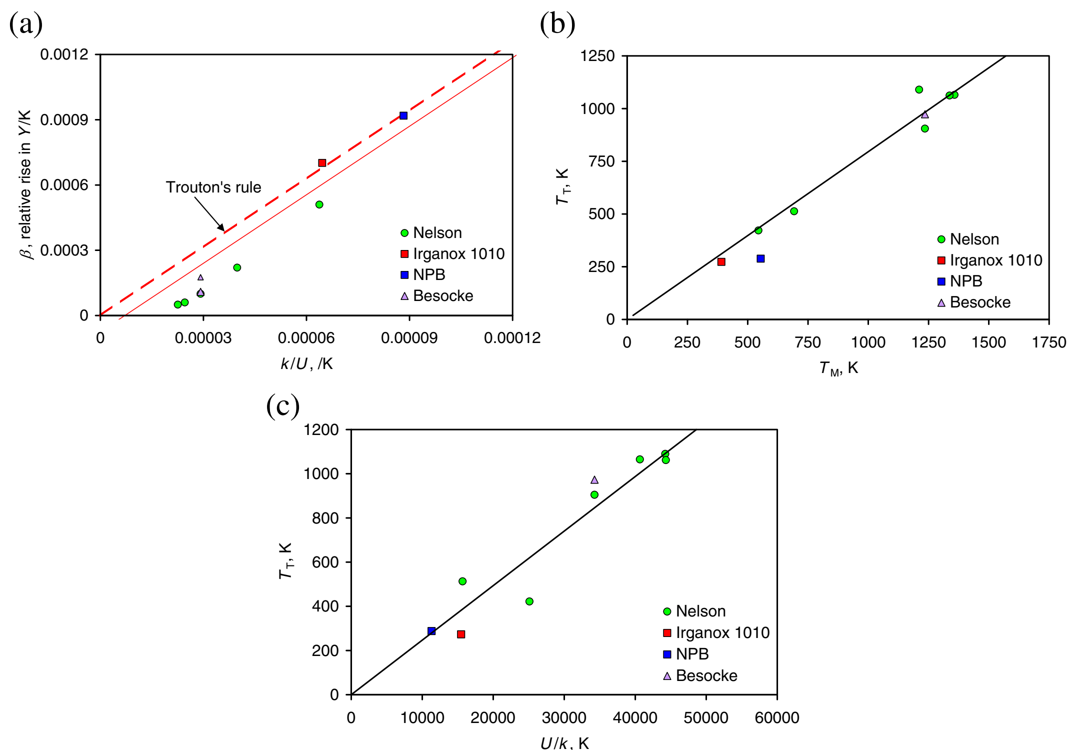

Figure 4. Temperature effects on the sputtering yields of metals from Nelson's (green circle) and Besocke et al's studies (purple triangle) as well as for Irganox 1010 (red square) and NPB (blue square), **(a)** the relative rate of increase of yield with temperature for low temperatures versus k/U, **(b)** the transition temperature, T_T versus the melting temperature, T_M, and **(c)** T_T versus U/k. The solid red line in **(a)** is for Trouton's rule and the dashed red line allows for the expansion coefficient. In **(b)** and **(c)**, the solid lines are linear regression fits to Nelson's data, passing through the origin

to that obtained for metals under a very different sputtering regime. We consider, next, the depth resolutions from the delta layers.

Depth Resolution

The depth resolutions may be determined via the observed FWHM of the delta layers or via λ_u, σ or λ_d in the component parts of the fits to the data. Figure 5 shows the FWHM results for the first delta layer. The behaviors of all component parts are consistent with these.

Note that the measure of depth resolution, 16% to 84%, given by Niehuis et al. [3] will lead to slightly smaller values than the FWHMs here. In both NPB and Irganox 1010 there is a significant reduction in FWHM once the temperature rises above T_T. This behavior would be consistent with a temporary local melting or surface diffusion where the sputtered crater and its rim anneal slightly before freezing, so partially flattening them. This is not an effect on the delta layers themselves since cooling to low temperatures after heating to 25 °C for Irganox 1010 and 50 °C for NPB gives the depth resolution appropriate to that lower temperature. Furthermore, the shelf life of both samples is significantly in excess of 6 mo at 25 °C without degradation. It is clear, however, that at 50 °C in the Irganox sample, the Irganox 3114 is still present but is now distributed more evenly through the sample, indicating that significant bulk interdiffusion has occurred at the higher temperatures. The Irganox 1010 is still stable, and the depth profile at 50 °C shows an excellent FWHM of 8.5 nm at the Si interface at 380 nm depth. It is surprising, therefore, not to see more diffusion at 25 °C when the diffusion distance must be of the order of 50 nm at 50 °C. At 25 °C, the diffusion distance must be less than 4 nm and probably significantly less than this. For the diffusivity to increase by at least $(50/4)^2 = 150$ times over a 25 °C rise in temperature would require the activation energy, Q, to exceed significantly, 1.5 eV per molecule. This is very likely in view of the interlocking nature of the Irganox 1010 molecules and the large cross section of the Irganox 3114

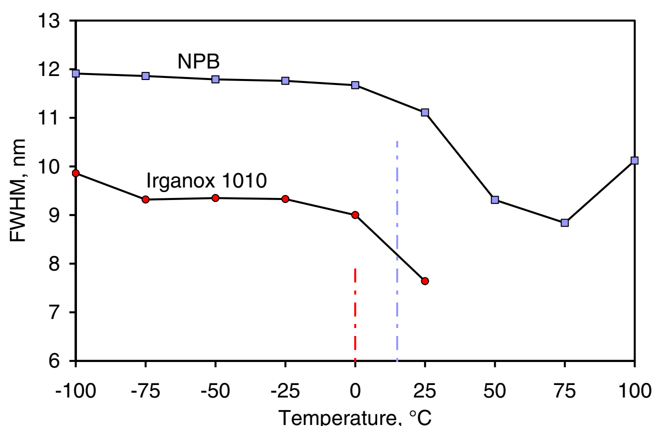

Figure 5. Five keV Ar_{2000}^+ FWHMs as a function of sample temperature for both NPB and Irganox 1010. The vertical lines show the T_T values

molecules but would require the high value of 50 for G in van Liempt's equation

$$Q = GRT_M \qquad (2)$$

where R is the gas constant and G is given as 10 to 35 by Brown and Ashby [41] and averages 17 for Mehrer [42] for self diffusion in elemental solids. Any movement of species is to be avoided even though the annealing of craters just above the transition temperature appear to be beneficial from a topographical point of view. It is recommended for the most consistent work that profiles are, therefore, conducted at temperatures significantly below $0.8T_M$, which, for many organic materials, will be below room temperature.

The interdiffusion observed at the higher temperatures is important for studying device degradation. The matrix has, in both cases, remained stable but the delta layer may no longer retain its original form. SIMS is an excellent method for studying this onset of degradation.

Spectra

In this study, the sputtering is done with 5 keV Ar_{2000}^+ primary ions and the analysis is done with 25 keV Bi_3^+. Both ions see the samples at the elevated or reduced temperatures and we can learn much from the SIMS spectra and their changes with temperature. For this purpose, spectra reconstructed from scans between the second and the third marker layer are analyzed. This excludes any secondary ions arising from the delta layers, contamination of the surface of the films, and ions from the silicon substrate. It is important to evaluate any compositional or other changes with increasing temperature. NPB and Irganox 1010 SIMS spectra may be found elsewhere and so are not given here [43]. The spectra for all temperatures are basically very similar and show no signs of decomposition or other significant changes except as discussed below. Figure 6 shows the change in the NPB monomer yield, Y_M, for the Bi_3^+ analysis ions as a function of the sputtering yield for the argon clusters. Elsewhere [44], we show that the sputtering yields for Bi_3^+ and argon clusters are similar at similar energies. We assume that their behaviors with temperature are similar. We calculate, for each spectrum, the total ion yield volume (TIYV) [44] and then scale the spectrum so that the TIYV is then proportional to the measured sputtering yield at that temperature. This reduces any scatter arising from repeatability in the sample positioning and the Bi beam currents. Figure 6a shows that $Y_M \propto Y^{0.46}$. This may be interpreted as, at the higher temperatures, the monomer secondary ions are emitted from a smaller fraction of the sputtered volume. For many ion fragments, the depth of emission comes from significantly less than the full crater depth [45]. If the craters at different temperatures all have a similar shape, emission that comes from a thin defined layer at the surface will vary as $Y^{(2/3)}$, whereas emission that comes from a defined rim zone will vary as $Y^{(1/3)}$. The monomer shows a power, s, between these two and is consistent with emission from a zone near the cooler rim. This shows that small changes are expected in the spectra arising from the

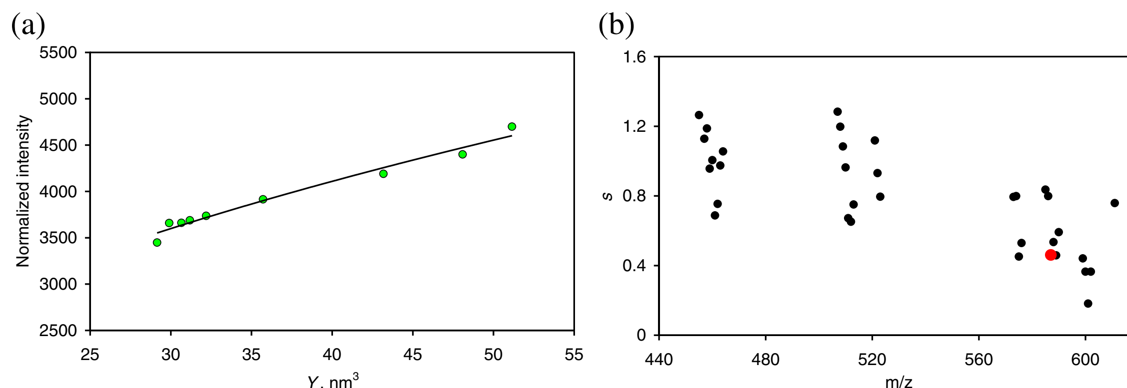

Figure 6. **(a)** Yield, Y_M, of the NPB monomer ion as a function of the sputtering yield Y at various temperatures. The solid line shows $Y_M \propto Y^{0.46}$, **(b)** the power dependence, s, for $Y_M \propto Y^s$ for near-monomer secondary ions. In **(b)**, the red dot is for the 587 Da ion shown in **(a)**

fractional contribution of the region of the crater from which specific ions arise. This change, although increasing the monomer signal as the temperature rises, does not increase it as fast as the increase for smaller fragments—the monomer signal weakens relative to those of the other ions.

If the above is correct, it would be expected that slightly damaged monomer entities would be generated from relatively larger regions and that, therefore, the above power would rise to unity for lower mass fragments (actually slightly above unity since the normalization makes the volume weighted average unity). This is what is observed, as shown by the power indexes for these ions in Figure 6b. The even lower power for the 601 Da entity is for the $(M + CH_2)^-$ ion, and probably arises from the reducing molecular interaction as the temperature increases. Thus, there are spectral changes but they are all weak and are associated with the sputtering process and not from any decomposition or other significant change in property.

The Irganox 1010 data only go up to 25 °C since, at higher temperatures, the depth resolution degraded so that the exact dose of the deeper layers became uncertain. The behaviors here are similar to those for NPB.

Above the transition temperature, the rate of increase of the sputtering yield rises by about an order of magnitude. As with polymers, a doubling of the sputtering rate may be observed. This similarity is surprising in view of the very different mechanisms proposed for polymers [18, 19]. Negative secondary ion spectra are measured, and these show significant systematic changes in which the fractional intensity of molecular entities decrease relative to those of the intermediately sized ion fragments. This is interpreted as their arising from near the edge of the crater. During the profiling, the depth resolutions are observed to change little below T_T but at higher temperatures the resolution improves at first and then degrades. The improvement may be associated with local melting or surface diffusion around the crater but the temperature to achieve this small advantage will vary from material to material and will be difficult to find. At a slightly higher temperature, bulk diffusion occurs and the sought-after structure is lost. It is therefore recommended that in general, the higher temperature zone is not used, and for the most consistent work, that profiles are conducted at temperatures significantly below T_T, which for many organic materials will be below room temperature. Adjustments to the sputtering yields [25] may be made using Trouton's rule.

Conclusions

It is shown that in depth profiling NPB and Irganox 1010 using 5 keV Ar_{2000}^+, the sputtering yields increase linearly with temperature from –100 °C up to a transition temperature, T_T, which is 15 °C for NPB and 0 °C for Irganox 1010. The rate of increase in this range is consistent with the data for metals by Nelson [31], and all data are consistent with the yield being inversely proportional to the temperature-dependent binding energy according to Trouton's rule. This is consistent with the universal sputtering equation [25, 44]. The transition temperature is approximately given by $0.8T_M$, where T_M is the melting temperature in Kelvin. This simple rule is easy to use with organic materials where many parameters are unknown but usually T_M is known.

Acknowledgments

The authors thank A. G. Shard, S. J. Spencer, and S. Smith for the samples used in this study. This work forms part of 3D nanoSIMS project in the Strategic Capability Program of the National Measurement System of the UK Department of Business, Innovation, and Skills, and the 14IND01-3DMetChemIT project in the EMPIR program cofinanced by the Participating States and from European Union's Horizon 2020 research and innovation program.

References

1. Gilmore, I.S.: SIMS of organics—advances in 2D and 3D imaging and future outlook. J. Vac. Sci. Technol. A **31**, 050819-1–050819-14 (2013)

2. Bich, C., Havelund, R., Moellers, R., Touboul, D., Kollmer, F., Niehuis, E., Gilmore, I.S., Brunelle, A.: Argon cluster source evaluation on lipid standards and rat brain tissue samples. Anal. Chem. **85**, 7745–7752 (2013)
3. Niehuis, E., Möllers, R., Rading, D., Cramer, H.-G., Kersting, R.: Analysis of organic multilayers and 3D structures using Ar cluster ions. Surf. Interface Anal. **45**, 158–162 (2013)
4. Tian, H., Wucher, A., Winograd, N.: Molecular imaging of biological tissue using gas cluster ions. Surf. Interface Anal. **46**, 115–117 (2014)
5. Yang, J., Gilmore, I.S.: Application of secondary ion mass spectrometry to biomaterials, proteins and cells: a concise review. Mater. Sci. Technol. **31**, 131–136 (2015)
6. Winograd, N.: Imaging mass spectrometry on the nanoscale with cluster ion beams. Anal. Chem. **87**, 328–333 (2015)
7. Aizawa, N., Pu, Y.-J., Watanabe, M., Chiba, T., Ideta, K., Toyota, N., Igarashi, M., Suzuri, Y., Sasabe, H., Kido, J.: Solution-processed multilayer small-molecule light-emitting devices with high-efficiency white-light emission. Nat. Commun. **5**, Art No 5756 (2014)
8. Matsuo, J., Ninomiya, S., Nakata, Y., Honda, Y., Ichiki, K., Seki, T., Aoki, T.: What cluster size is most appropriate for SIMS. Appl. Surf. Sci. **255**, 1235–1238 (2008)
9. Shard, A.G., Green, F.M., Brewer, P.J., Seah, M.P., Gilmore, I.S.: Quantitative molecular depth profiling of organic delta layers by C_{60} ion sputtering and SIMS. J. Phys. Chem. B **112**, 2596–2605 (2008)
10. Shard, A.G., Havelund, R., Seah, M.P., Spencer, S.J., Gilmore, I.S., Winograd, N., Mao, D., Miyayama, T., Niehuis, E., Rading, D., Moellers, R.: Argon cluster ion beams for organic depth profiling: results from a VAMAS interlaboratory study. Anal. Chem. **84**, 7865–7873 (2012)
11. Lee, J.L.S., Ninomiya, S., Matsuo, J., Gilmore, I.S., Seah, M.P., Shard, A.G.: Organic depth profiling of a nanostructured delta layer reference material using large argon cluster ions. Anal. Chem. **82**, 98–105 (2010)
12. Dowsett, M.G., Rowlands, G., Allen, P.N., Barlow, R.D.: An analytic form for the SIMS response function measured from ultra-thin impurity layers. Surf. Interface Anal. **21**, 310–315 (1994)
13. Green, F.M., Shard, A.G., Gilmore, I.S., Seah, M.P.: Analysis of the interface and its position in C_{60}^{n+} secondary ion mass spectrometry depth profiling. Anal. Chem. **81**, 75–79 (2009)
14. Green, F.M., Seah, M.P., Gilmore, I.S., Salter, T.L., Spencer, S.J.: Analysis of thin films and molecular orientation using cluster SIMS. Surf. Interface Anal. **43**, 1224–1230 (2011)
15. Seah, M.P.: Measurement of the roughness of unannealed and annealed surfaces by atomic force microscopy. Meas. Sci. Technol. **25**, 105001–105013 (2014)
16. Mahoney, C.M.: Cluster secondary ion mass spectrometry of polymers and related materials. Mass Spectrom. Rev. **29**, 247–293 (2010)
17. Mahoney, C.M., Fahey, A.J., Gillen, G., Xu, C., Batteas, J.D.: Temperature-controlled depth profiling in polymeric materials using cluster secondary ion mass spectrometry (SIMS). App. Surf. Sci. **252**, 6502–6505 (2006)
18. Mahoney, C.M., Fahey, A.J., Gillen, G.: Temperature-controlled depth profiling of poly(methyl methacrylate) using cluster secondary ion mass spectrometry. 1. Investigation of depth profile characteristics. Anal. Chem. **79**, 828–836 (2007)
19. Mahoney, C.M., Fahey, A.J., Gillen, G., Xu, C., Batteas, J.D.: Temperature-controlled depth profiling of poly(methyl methacrylate) using cluster secondary ion mass spectrometry. 2. Investigation of sputter-induced topography, chemical damage, and depolymerization effects. Anal. Chem. **79**, 837–845 (2007)
20. Cristaudo, V., Poleuris, C., Czerwinski, B., Delcorte, A.: Ar Cluster sputtering of polymers: effects of cluster size and molecular weights. Surf. Interface Anal. **46**(S1), 79–82 (2014) and **46**(S1) 405 (2014)
21. Seah, M.P.: Argon cluster size-dependence of sputtering yields of polymers: molecular weights and the universal equation. Surf. Interface Anal. **47**, 169–172 (2015)
22. Möllers, R., Tuccitto, N., Torrisi, V., Niehuis, E., Licciardello, A.: Chemical effects in c60 irradiation of polymers. App. Surf. Sci. **252**, 6509–6512 (2006)
23. Dowsett, M.G., Kelly, J.H., Rowlands, G., Ormsby, T.J., Guzmán, B., Augustus, P., Beanland, R.: On determining accurate positions, separations, and internal profiles for delta layers. App. Surf. Sci. **203/204**, 273–276 (2003)
24. Seah, M.P., Havelund, R., Shard, A.G., Gilmore, I.S.: Sputtering yields for mixtures of organic materials using argon gas cluster ions. J. Phys. Chem. B **119**, 13433–13439 (2015)
25. Seah, M.P.: Universal equation for argon gas cluster sputtering yields. J. Phys. Chem. C **117**, 12622–12632 (2013)
26. Holzweber, M., Shard, A.G., Jungnickel, H., Luch, A., Unger, W.E.S.: Dual beam organic depth profiling using large argon cluster ion beams. Surf. Interface Anal. **46**, 936–939 (2014)
27. Seah, M.P., Spencer, S.J., Havelund, R., Gilmore, I.S., Shard, A.G.: Depth resolution at organic interfaces sputtered by argon gas cluster ions: the effect of energy, angle, and cluster size. Analyst **140**, 6508–6516 (2015)
28. Seah, M.P., Clifford, C.A., Green, F.M., Gilmore, I.S.: An accurate semi-empirical equation for sputtering yields, I: for argon ions. Surf. Interface Anal. **37**, 444–458 (2005)
29. Seah, M.P.: An accurate semi-empirical equation for sputtering yields, II: for neon, argon, and xenon ions. Nucl. Instrum. Methods B **229**, 348–358 (2005)
30. Yamada, I., Matsuo, J., Toyoda, N., Kirkpatrick, A.: Materials processing by gas cluster ion beams. Mater. Sci. Eng. R **34**, 231–295 (2001)
31. Nelson, R.S.: An Investigation of thermal spikes by studying the high energy sputtering of metals at elevated temperatures. Philos. Mag. **11**, 291–302 (1965)
32. Carlston, C.E., Magnuson, G.D., Corneaux, A., Mahadevan, P.: Effect of elevated temperatures on sputtering yields. Phys. Rev. **138**, A759–A763 (1965)
33. Eckstein, W.: In: Behrisch, R., Eckstein, W. (eds.) Sputtering yields, Chapter 3 in sputtering by particle bombardment, pp. 33–187. Springer, Berlin (2007)
34. Besocke, K., Berger, S., Hofer, W.O., Littmark, U.: A Search for a thermal spike effect in sputtering. Rad. Effects **66**, 35–41 (1982)
35. Trouton, F.T.: On molecular latent heat. Philos. Mag. **18**, 54–57 (1884)
36. Kubaschewski, O., Evans, E.L., Alcock, C.B.: Metallurgical thermochemistry, 4th edn. Pergamon, Oxford (1967)
37. Mishra, D.S., Yalkowsky, S.H.: Estimation of entropy of vaporization: effect of chain length. Chemosphere **21**, 111–117 (1990)
38. Luwei, Z., Na, N., Yalkowsky, S.H.: A modification of Trouton's rule by simple molecular parameters for hydrocarbon compounds. Ind. Eng. Chem. Res. **38**(1), 324–327 (1999)
39. Kaye, G.W.C., Laby, T.H.: Tables of physical and chemical constants, 16th ed. Longman: Harlow (1995) and also online, available at http://www.kayelaby.npl.co.uk. Accessed 15 April 2016
40. Walters, A.E., Myrdal, P.B., Yalkowsky, S.H.: A method for estimating the boiling points of organic compounds from their melting points. Chemosphere **31**, 3001–3008 (1995)
41. Brown, A.M., Ashby, M.F.: Correlations for diffusion constants. Acta Met **28**, 1085–1101 (1980)
42. Mehrer, H.: Springer series in solid state science 155, diffusion in solids, fundamentals, methods, materials, diffusion-controlled processes, chap 8, pp. 141–147. Springer, Berlin (2007)
43. Seah, M.P., Green, F.M., Gilmore, I.S.: Cluster primary ion sputtering: secondary ion intensities in static SIMS of organic materials. J. Phys. Chem. C **114**, 5351–5359 (2010)
44. Seah, M.P., Havelund, R., Gilmore, I.S.: Universal equation for argon cluster size dependence of secondary ion spectra in SIMS of organic materials. J. Phys. Chem. C **118**, 12862–12872 (2014)
45. Havelund, R., Seah, M.P., Gilmore, I.S.: Sampling depths, depth shifts, and depth resolutions for Bi_n^+ ion analysis in argon gas cluster depth profiles. J. Phys. Chem. B **120**, 2604–2611 (2016)